HHS Public Access

Author manuscript

Cell. Author manuscript; available in PMC 2015 December 18.

Published in final edited form as:

Cell. 2014 December 18; 159(7): 1603–1614. doi:10.1016/j.cell.2014.11.025.

Acetate is a Bioenergetic Substrate for Human Glioblastoma and Brain Metastases

Tomoyuki Mashimo[1,2,3,11], **Kumar Pichumani**[4,11], **Vamsidhara Vemireddy**[1,2,3], **Kimmo J. Hatanpaa**[2,3,5], **Dinesh Kumar Singh**[2,3,6], **Shyam Sirasanagandla**[1,2,3], **Suraj Nannepaga**[2,3,6], **Sara G. Piccirillo**[3,6], **Zoltan Kovacs**[4], **Chan Foong**[5], **Zhiguang Huang**[7], **Samuel Barnett**[8], **Bruce E. Mickey**[2,3,8], **Ralph J. DeBerardinis**[2,9,10], **Benjamin P. Tu**[7], **Elizabeth A. Maher**[1,2,3,6,12], and **Robert M. Bachoo**[1,2,3,6,12]

[1]Department of Internal Medicine, UT Southwestern Medical Center, Dallas, Texas 75390

[2]Simmons Comprehensive Cancer Center, UT Southwestern Medical Center, Dallas, Texas 75390

[3]Annette G. Strauss Center for Neuro-Oncology, UT Southwestern Medical Center, Dallas, Texas 75390

[4]Advanced Imaging Research Center, UT Southwestern Medical Center, Dallas, Texas 75390

[5]Department of Pathology, UT Southwestern Medical Center, Dallas, Texas 75390

[6]Department of Neurology and Neurotherapeutics, UT Southwestern Medical Center, Dallas, Texas 75390

[7]Department of Biochemistry, UT Southwestern Medical Center, Dallas, Texas 75390

[8]Department of Neurological Surgery, UT Southwestern Medical Center, Dallas, Texas 75390

[9]McDermott Center for Human Growth and Development, UT Southwestern Medical Center, Dallas, Texas 75390

[10]Children's Medical Center Research Institute, UT Southwestern Medical Center, Dallas, Texas 75390

Abstract

Correspondence: Robert.bachoo@utsouthwestern.edu, Elizabeth.maher@utsouthwestern.edu.
[11]Co-first author,
[12]Co-senior author

AUTHOR CONTRIBUTIONS

The study was conceived by EAM and RMB. TM managed all the HOT lines, infusion experiments and tissue samples. VV did the cannulations and infusions as well as all the IHC and analysis of TMAs. VV, SS, SN, DS did the orthotopic injections. DS performed the ACSS2 expression studies. KP did the NMR runs and spectral analysis. KH and CF developed the TMA and KH performed the analysis. ZH and BPT performed the MEF experiments. SP generated the GBM cultures and performed the shRNAi experiments. BEM and SB are did the patient surgical procedures and obtained tumor tissue. RJD, KP, BPT, EAM and RMB performed the integrated analysis and wrote the paper.

Glioblastomas and brain metastases are highly proliferative brain tumors with short survival times. Previously, using ^{13}C-NMR analysis of brain tumors resected from patients during infusion of ^{13}C-glucose, we demonstrated that there is robust oxidation of glucose in the citric acid cycle, yet glucose contributes less than 50% of the carbons to the acetyl-CoA pool. Here we show that primary and metastatic mouse orthotopic brain tumors have the capacity to oxidize [1,2-^{13}C]acetate and can do so simultaneously with [1,6-^{13}C]glucose oxidation. The tumors do not oxidize [U-^{13}C]glutamine. In vivo oxidation of [1,2-^{13}C]acetate was validated in brain tumor patients and was correlated with expression of acetyl-CoA synthetase enzyme 2, ACSS2. Together the data demonstrate a strikingly common metabolic phenotype in diverse brain tumors that includes the ability to oxidize acetate in the citric acid cycle. This adaptation may be important for meeting the high biosynthetic and bioenergetic demands of malignant growth.

INTRODUCTION

Malignant brain tumors are among the most intractable problems in cancer. Glioblastoma (GBM), the most common and aggressive primary tumor has a median survival of 15 months. Despite intense clinical efforts at targeting various signaling pathways, putative driver mutations, and angiogenesis mechanisms, no improvement in survival has emerged since the addition of temozolomide to radiation as initial therapy in 2005 (Fine, 2014). Brain metastases, similarly, are aggressive tumors that affect ~200,000 patients per year in the United States (Lu-Emerson and Eichler, 2012) and usually occur late in the clinical course, often heralding end-stage disease. Treatment options are limited and survival is measured in months (Owonikoko et al., 2014). Although GBM and brain metastases represent a broad range of cancer subtypes with distinct cellular origins and diverse genetic programs, they exhibit common metabolic characteristics that may be the result of reprogramming to enable rapid growth in the brain. Using ^{13}C-NMR we have previously shown in patients with GBM, lung and breast cancer brain metastases that these tumors oxidize glucose in the citric acid cycle (CAC) to produce macromolecular precursors and energy (Maher et al., 2012). The metabolic complexity of these tumors is further reflected in the identification of a ‘bioenergetic substrate gap’, whereby a significant fraction of the acetyl-CoA pool is not derived from blood-borne glucose (Maher et al., 2012). The striking commonality of this finding among different grades of gliomas and metastatic tumors of diverse cellular origins prompted us to consider the possibility that an alternate or additional substrate(s) may serve an important carbon source for generating CAC intermediates to support biosynthesis and bioenergetics *in vivo*.

Although the normal healthy adult brain relies almost exclusively on glucose as the major energy substrate, it can readily adapt to alternate fuels, including ketone bodies, short and medium chain fatty acids and acetate (Ebert et al., 2003). Astrocytes are capable of supporting neuronal function by utilizing acetate as a metabolic substrate under conditions of limiting glucose supply including diabetic hypoglycemia and chronic alcohol abuse (Jiang et al., 2013; Schurr, 2001). Since GBMs develop from the astro-glial lineage, we hypothesized that these tumors retain the capacity to metabolize acetate during transformation. The most common brain metastases, in contrast, arise from organs that are not known to utilize substrates other than glucose. We speculated, however, that the unique

brain microenvironment might drive tumors of diverse origins to utilize the same metabolic substrates to fuel aggressive growth. To test this hypothesis *in vivo* we used human orthotopic tumor (HOT) mouse models of GBM and brain metastases and applied methods in intermediary metabolism for studying multiple substrates using ^{13}C-labeled nutrients (Malloy et al., 1988; Sherry et al., 1992). Co-infusion of ^{13}C-acetate and ^{13}C-glucose has been used extensively to study normal rodent brain metabolism in which differential handling of acetate and glucose by the glial and neuronal compartments can be demonstrated by ^{13}C-NMR of resected brain tissue. These methods enable direct tracing of the metabolic fate of infused substrates beyond simple uptake in the cell and therefore can be used to determine directly whether acetate can be oxidized by GBM and/or brain metastases in an orthotopic model *in vivo*.

Here we report that mice harboring human GBM or brain metastases can completely oxidize acetate in the tumors. We have validated this finding in patient tumors by infusing ^{13}C-acetate in patients with GBM, breast cancer and non-small cell lung cancer during surgical resection of their tumors and show that there is robust labeling of CAC intermediates by blood-borne ^{13}C-acetate.

In the accompanying manuscript by Comerford et al. (2014), the authors demonstrate a critical role for the nucleo-cytosolic acetyl-CoA synthetase enzyme, ACSS2, in hepatocellular carcinoma and broad immunoreactivity for ACSS2 in diverse human tumor types including gliomas, breast cancer and lung cancer. Here we show that ACSS2 is upregulated in the HOT and primary human tumors, as well as a murine glioma model. In ACSS2 knockout mouse embryo fibroblasts (MEFs), ^{13}C-acetate fails to label CAC intermediates and in human GBM neurospheres, stable ACSS2 knockdown leads to failure of self-renewal. These studies provide a potential mechanistic link between ACSS2 activity and *in vivo* acetate oxidation in tumors.

RESULTS

Glioblastomas oxidize acetate in the citric acid cycle

The human orthotopic tumor (HOT) lines of GBM and brain metastases used in this study were each derived from an individual patient tumor, implanted into the basal ganglia of NOD-SCID mice within 3 hours of surgical resection. Clinically symptomatic tumors were generated within 2–4 months. The tumors, which are linked to IRB-approved collection of clinical information, were serially passaged and expanded in the mouse brain without adaptation to cell culture. This helps ensure preservation of the phenotypic, molecular, and metabolic profiles of the human tumors and tumor-stromal interactions, to the extent possible in an experimental system. We selected 6 HOT lines (UT-GBM1–6, Table S1) that are representative of the most common GBM molecular profiles (Brennan et al., 2013). Each line was generated at the time of the patient's initial diagnosis prior to any treatment and was studied here in early *in vivo* passage. A 7th HOT line (UT-GBM7), generated at the time of repeat surgery for tumor recurrence 15 months after initial resection in the same patient that the UT-GBM6 HOT line was derived from, was chosen to compare substrate utilization in the setting of recurrence and multi-modality resistance. We have validated *in vivo* that UT-

GBM6 is temozolomide (TMZ) sensitive while UT-GBM7 is TMZ resistant (Sagiyama et al., 2014).

Representative histological sections from UT-GBM1 (Figure 1A) show an expansive mass (T) comprised of densely packed tumor cells and infiltration into brain at the leading edges. In each mouse the contralateral hemisphere served as a matched control for substrate utilization. It is referred to as 'non-tumor bearing brain' (NT, Figures 1A) rather than 'normal brain' because the brain surrounding a large tumor is subjected to mass effect, an increase in reactive astrocytes, and diffusible factors from the tumor and/or blood; conditions which could potentially impact brain metabolism. ^{13}C-NMR analysis of NT brain provides a valuable internal control for each mouse since the NT and T are exposed to the same circulating concentrations of ^{13}C-glucose and ^{13}C-acetate and systemic conditions of the mouse. Thus, differences in labeling patterns and substrate utilization between NT and T reflect tumor-specific handling of the substrates.

[1,6-^{13}C]glucose and [1,2-^{13}C]acetate were chosen for co-infusion because oxidation of each substrate has been shown to produce distinct labeling patterns in CAC intermediates enabling a direct comparison of substrate utilization in a given tissue (Deelchand et al., 2009; Malloy et al., 1988; Taylor et al., 1996). In the schema (Figure 1B), metabolism of [1,6-^{13}C]glucose (blue circles) leads to labeling of carbon 3 in pyruvate, followed by production of acetyl-CoA labeled in position 2 which condenses with oxaloacetate (OAA) leading to labeling of carbon 4 in α-ketoglutarate (α-KG), glutamate and glutamine during the first turn of the CAC, and in carbons 3 and 4 with subsequent turns. This generates a singlet (S) and doublet 3, 4 (D34) in Glutamate C4 (GLU4) and Glutamine C4 (GLN4) (example, Figure 1C). In contrast, metabolism of [1,2-^{13}C]acetate leads to labeling of both carbons (red circles) of acetyl-CoA with subsequent labeling of carbons 4 and 5 of α-KG and glutamate in the first turn of the CAC, generating a doublet 4,5 (D45) (example, Figure 1C). In subsequent turns of the cycle, labeling in carbons 3,4, and 5 generates a doublet of doublets (quartet, Q) (example Figure 2A). Thus, the ^{13}C-NMR multiplet pattern in carbon 4 of glutamate (GLU4) reflects differential labeling of the acetyl-CoA pool and provides a direct and unequivocal readout of substrate metabolism; D45 and Qs reporting acetate oxidation and S and D34 reporting glucose oxidation (Sherry et al., 1992). The fractional amount of each multiplet in GLU4 can be obtained by determining the area of each multiplet relative to the total spectral area of GLU4 in which the areas of S, D34, D45, and Q sum to 1 (Marin-Valencia et al., 2012b).

The NT brain ^{13}C-NMR spectrum (Figure 1C) shows high signal to noise and well resolved multiplets arising from ^{13}C-^{13}C coupling. Oxidation of both glucose and acetate in NT brain is demonstrated by the presence of S and D34 from glucose and D45 from acetate in GLU4 (Figure 1C inset). Although the same multiplets are present in Glutamine C4 (GLN4), the pattern of D45 and D34 is different than in GLU4, recapitulating the pattern that results from the differential handling of acetate and glucose in glia and neurons (Taylor et al., 1996). The ^{13}C-NMR tumor spectrum from the same mouse (Figure 2A inset) has several notable differences. First, there is a marked increase in D45 and the appearance of Qs, indicating increased oxidation of acetate in the tumor when compared to the NT brain.

Second, the similarity between the GLU4 and GLN4 labeling pattern (prominent D45 and small D34) provides evidence that glutamine is being derived from glutamate in the tumor.

To determine the biological variability of acetate utilization within individual mice with tumors derived from the same parental line (UT-GBM1), we co-infused an additional 4 mice. The resulting ^{13}C-NMR spectral patterns of GLU4 and GLN4 in NT brain and tumor were almost indistinguishable from the NT brain and tumor spectra in Figures 2A and 2B (data not shown). To quantify the relative contribution of each substrate to the labeling in GLU4, we calculated the acetate:glucose ratio (D45+Q):(S+D34). This has been used extensively in brain metabolism where the differential labeling of multiplets enables discrimination of glial and neuronal metabolism, since astrocytes, but not neurons, are capable of oxidizing acetate (Deelchand et al., 2009; Marin-Valencia et al., 2012b). In applying this analysis to brain tumors, we assume a single compartment comprised of tumor cells, based on histological analysis. Thus, the acetate:glucose ratio in tumor GLU4 reflects the relative contribution of each labeled substrate. The ratio was calculated for the 5 mice, NT brain and tumor (Figure 2B).

In NT brain, glucose is the major substrate being oxidized with an acetate:glucose ratio of 15.8+/−1.2% : 84.2+/−1.1% (ratio 0.19+/−0.02), achieved with fractional enrichment of ^{13}C-glucose of 32+/−5% in the blood and plasma acetate levels that rose approximately 4 fold (from 0.177 +/− 0.02 mM to 0.619 +/− 0.13 mM) during infusion. The ratio is remarkably similar to the published report of acetate:glucose ratio in normal adult mouse brain (calculated as 14%:86%,ratio 0.16, (Marin-Valencia et al., 2012b). The acetate:glucose ratio in the 5 tumors was 51.8+/−2.9% : 48.3+/−2.9% (ratio 1.02+/−0.09), 5 fold higher than in NT brain ($p<0.001$), demonstrating a significant shift toward acetate oxidation in the tumor.

Direct analysis of the multiplet ratios in GLU4 does not provide information about the contribution of unlabeled substrates in the acetyl-CoA pool, which could be playing an important role in fueling the tumor. To determine the unlabeled pool, we applied a validated non-steady state algorithm to the spectral analysis, which takes into account the total multiplet area in the glutamate C3 and C4 and the levels of infused substrates in the blood (Malloy et al., 1988; Malloy et al., 1990b). The fraction of acetyl-CoA due to acetate increased from 6.0+/−1.2% in NT brain to 24.7+/−2% in the tumor ($p<0.0001$). This was associated with a decrease in the fractional contribution from glucose from 75.8+/−3.7% in NT brain to 50.4+/−9.1% in the tumor ($p<0.002$), while the unlabeled fraction was not significantly different between NT brain (18.2+/−4.0%) and tumor (25.5+/−8.0%). The decrease in glucose oxidation between NT brain and tumor may, at least in part, reflect a loss of the neuronal contribution to glucose utilization.

Having established the reproducibility of biological replicates in UT-GBM1 that has PDGFR overexpression/PTEN deletion, we next addressed the question of whether the ability to oxidize acetate is a function of the dominant oncogenes and/or tumor suppressor genes in the tumor. Mice from five additional GBM HOT lines (UT-GBM2-6, Supplemental Table 1) were co-infused with [1,2-^{13}C]acetate and [1,6-^{13}C]glucose. The acetate:glucose ratios were calculated for these lines. No differences were found among the NT brains and

in each line tumor acetate oxidation was higher than in NT brain. The relative ^{13}C-acetate contribution to GLU4 ranged from 18.8% to 52% (32+/−5%) in the tumor. Differences in the percent acetate oxidation among the individual lines could not be attributed to amplification of EGFR or PDGFRα, presence of the EGFR VIII mutant, loss of PTEN or loss of INK4a/ARF (data not shown).

Since all 6 GBM HOT lines were generated from patient tumors prior to the initiation of treatment, we next examined the tumor line generated from recurrent tumor (UT-GBM7) and compared it directly with the initial GBM HOT line from the same patient (UT-GBM6). Nearly identical labeling patterns in GLU4 and GLN4 were identified (Figure S1), with dominance of the D45, an acetate:glucose ratio 25%:75% in the initial tumor (UT-GBM6) and 27%:73% in the recurrent tumor (UT-GBM7). The relative avidity for acetate and glucose is remarkably similar in these tumors that were derived independently more than a year apart and after extensive treatment and acquisition of chemo- and radioresistance.

Brain Metastases from Diverse Cell Types Oxidize Acetate

To determine whether acetate oxidation is a feature of non-glial brain tumors, we studied 5 brain metastasis HOT tumor lines; breast cancer (estrogen receptor (ER) and progesterone receptor (PR) negative, HER2 positive), non-small cell lung cancer (no mutations in EGFR, ALK, or KRAS), clear cell renal cell carcinoma (VHL−/−), melanoma (BRAF^{V600E} mutated) and endometrial cancer, a tumor which rarely metastasizes to the brain. There is remarkable preservation of the signature histopathological and molecular features of the human brain metastases in the HOT models (see examples Figure 3). Of note, the breast and lung cancer HOT lines were generated from the human tumors infused with ^{13}C-glucose during surgery that we reported previously (Maher et al., 2012), each of which oxidized glucose but also showed a significant bioenergetic substrate gap. The study of these tumors as orthotopic mouse models provided a unique opportunity to assess metabolic phenotype fidelity in these models.

The ^{13}C-NMR spectral patterns from the 5 individual tumor lines and matching NT brains following co-infusion of [1,6-^{13}C]glucose and [1,2-^{13}C]acetate recapitulated the findings in GBM with remarkable similarity. Representative GLU4 and GLN4 labeling from the breast cancer (Figure 3A) and melanoma (Figure 3B) reveal prominent D45 consistent with oxidation of acetate as well as a large singlet (S) and small D34, consistent with glucose oxidation. The acetate:glucose ratio in GLU4 was calculated for NT brain and tumor. Similar to the GBMs, there was a significant increase in the fraction of acetate being oxidized in the tumors, ranging from 21 to 42% (29+/−3%). Calculation of the fractional contribution to the acetyl-CoA pool for these tumors yielded 14.5+/−3.9% from ^{13}C-acetate, 49.2+/−5.6% from ^{13}C-glucose, and 37+/−4.3% from unlabeled substrate.

Glutamine is not directly oxidized in the CAC of GBM and brain metastases *in vivo*

We have previously shown that GBM HOT tumors do not oxidize glutamine in the CAC *in vivo* (Marin-Valencia et al., 2012c). Here we examined an additional 2 GBM HOT lines to increase the molecular diversity of the lines being examined and 3 brain metastasis HOT lines (non-small cell lung cancer, melanoma and endometrial cancer) to determine whether

glutamine could be directly oxidized in these tumors. Nearly identical spectra were obtained following infusion of [U-^{13}C]glutamine in the 3 tumor lines (Figure 3C, Figure S2A) and in GBM (data not shown). GLN4 was dominated by large Qs, which is consistent with the presence of ^{13}C-glutamine in the tumor, and the presence of smaller Qs in GLU4 suggests some exchange with [U-^{13}C]glutamate. However, GLU4 in each tumor was dominated by D45, a pattern that cannot be produced simply from direct exchange with glutamine. Moreover, prominent Qs in malate or aspartate were not visible in the spectra (Figure 3C), as would have been expected if [U-^{13}C]glutamine had exchanged with glutamate, which then exchanged with α-KG and ultimately was fully oxidized in the CAC. An alternative route for GLU4 ^{13}C labeling in the tumor was more likely. The multiplet patterns in lactate and alanine from liver, NT brain, and tumor from the lung metastasis HOT line (Figure S2B) are consistent with production of ^{13}C-glucose from infused [U-^{13}C]glutamine outside the CNS, likely in the liver, with subsequent ^{13}C-glucose oxidation in NT brain and tumor. This is supported by the presence of ^{13}C-labeled glucose in the liver ^{13}C-NMR spectrum (Figure S2C). Taken together, the labeling patterns in the HOT GBM and brain metastasis tumors following infusion of [U-^{13}C]glutamine further extends our previous finding in GBM that glutamine is taken up by the tumors but is not directly oxidized in the CAC *in vivo*.

ACSS2 upregulation is associated with more aggressive disease in glioma

ACSS2 is a critical enzyme for converting acetate to acetyl-CoA in murine models of liver cancer (Comerford et al., 2014) and was assessed here for a potential role in acetate metabolism in brain tumors. ACSS2 immunohistochemistry (IHC) showed moderate to high expression in 6 of 7 GBM and all brain metastasis HOT lines (Figure S3). It was notable that the GBM with the lowest fractional acetate oxidation (~18%) had the lowest ACSS2 expression by IHC (score=50). ACSS2 expression in our clinically annotated glioma tissue microarray (TMA) was variable (Figure 4A) but significantly higher in GBM than the grade II and II gliomas (Figure 4B). Among the grade II and III gliomas, shorter survival time was positively correlated with higher ACSS2 staining (Figure 4C). ACSS1, ACSS3, sterol regulatory element binding protein (SREBP-1) expression in the TMA was not correlated with ACSS2 expression or with survival in any of the clinical subgroups (data not shown).

To determine whether ACSS2 has a direct impact on GBM growth, primary neurosphere cultures derived from 2 independent GBM HOT lines were infected with retroviruses expressing an shRNAi targeting ACSS2 knockdown (KD) or a scrambled shRNAi (SCR). Comerford et al., 2014, have extensively characterized these retroviruses. Infection with ACSS2-KD shRNAi but not SCR resulted in cell death (Figure 5A). Surviving GBM cells failed to form neurospheres (2+/−0.5% vs 23+/−4%, $p<0.001$) and thus could not be assessed for *in vivo* tumorigenicity.

ACSS2 expression is associated with transformation and enables ^{13}C-acetate incorporation into glutamate

We next investigated whether ACSS2 has a potential role in glioma tumorigenicity. Primary astrocyte cultures were generated from multi-allele conditional mice carrying glioma-relevant mutations (p53$^{f/f}$, PTEN$^{f/f}$ and $_{LSL}$BRAF^{V600E}) that activate the PI3K/AKT and MAPK/ERK pathways. In this *ex vivo* model, successive mutations were associated with

increased ACSS2 expression, with the triple mutant cells, $p53^{-/-}$ $PTEN^{-/-}BRAF^{V600E}$, having the highest ACSS2 expression (Figure 5B). High-grade gliomas generated from intracranial implantation of the triple mutant cells were able to oxidize acetate when co-infused with ^{13}C-acetate and ^{13}C-glucose (Figure 5C). It is notable that, in contrast to the tumor suppressor-deficient, immortalized primary astrocytes, wild type astrocytes markedly downregulated expression of all ACSS enzymes under standard culture conditions (Figure 5D), making it an unreliable experimental system for further *in vitro* acetate metabolic studies.

To determine whether there is a direct mechanistic link between ACSS2 and oxidation of ^{13}C-acetate, we investigated the extent of ^{13}C-acetate incorporation into glutamate in ACSS2 KO MEFs. The KO MEFs exhibited very little incorporation of ^{13}C-acetate into glutamate, whereas re-introduction of the WT ACSS2 gene into these cells significantly increased acetate incorporation into glutamate (Figure S3). This direct genetic gain-of-function experiment provides a compelling link between ACSS2 and acetate oxidation in the CAC.

^{13}C-acetate is oxidized in patient brain tumors

To validate in humans the finding that acetate can be oxidized in the orthotopic models, we next infused [1,2-^{13}C]acetate in 4 patients (2 GBM, 1 breast cancer brain metastasis, 1 non-small cell lung cancer brain metastasis) during surgical resection of their tumors. Despite the diversity of tumor types, nearly identical ^{13}C-NMR spectra with excellent signal to noise ratio and robust labeling in glutamate and glutamine were obtained in the 4 tumors (Figures 6, 7, and Figure S4). The dominance of the D45 and presence of quartets (Q) in GLU4 and GLN4 is direct evidence that acetate was oxidized in the CAC. Moreover, the same multiplet pattern in glutamine demonstrates that this metabolite was generated from glutamate that had originated as blood-borne acetate. ^{13}C-acetate enrichment in the blood was 88.5+/−6.4%. Less than 3% (2.4+/−1.1%) ^{13}C-glucose was recovered in the blood, demonstrating that the labeling in the tumors was not due to ^{13}C-glucose production outside the CNS. The fractional contribution of [1,2-^{13}C]acetate to the acetyl-CoA pool in the 4 tumors was 47.8+/−3.8%. Unlabeled substrate accounted for 51.3+/−2.6% of the acetyl-CoA pool, with 1.7+/−0.4% coming from [2-^{13}C]acetate, consistent with natural abundance ^{13}C. The unlabeled fraction is likely due in large part to circulating glucose, based on data from our previous study of brain tumor patients infused with ^{13}C-glucose (Maher et al., 2012). ACSS2 immunoreactivity ranged from moderately to strongly positive in the 4 tumors, with specificity demonstrated in the lung brain metastasis (Figure 7) where tumor, but not surrounding stroma, is labeled.

DISCUSSION

Determining the carbon source(s) for biosynthesis and bioenergetics in rapidly proliferating tumors *in vivo* represents a critical step toward identifying potential vulnerabilities for therapeutic targeting. Our initial ^{13}C-NMR data from ^{13}C-glucose infusion in brain tumor patients (Maher et al., 2012) demonstrated a complex metabolic tumor phenotype that had not previously been reported; excess production of lactate (the Warburg effect) occurring

simultaneously with robust CAC oxidation of glucose as well as oxidation of another unidentified substrate(s), termed the 'bioenergetic substrate gap'. Here we show that brain tumors from widely diverse cellular origins have the capacity to oxidize infused ^{13}C-acetate. This finding in GBMs is perhaps not surprising given that glial cells, the presumptive GBM cells of origin, are well known to be capable of oxidizing acetate. This suggests that, despite the extensive molecular reprogramming that is a hallmark of GBM, the ability to oxidize acetate is preserved, if not enhanced, in the tumors. ^{11}C-acetate positron emission tomography (PET) positivity has been reported in gliomas (Yamamoto et al., 2008) consistent with our finding that acetate is actively taken up by the proliferating tumor cells. Nutrient uptake, however, while being of significant clinical utility as an imaging biomarker, provides no information about entry of the nutrient into specific metabolic pathways. A major advantage of ^{13}C-NMR, as demonstrated here, is that within a single spectrum there are multiple internal controls for examination of the relative activity of specific metabolic pathways. For example, the pyruvate pool is read out by labeling in lactate and alanine, while glutamate C4 reads out the acetyl CoA pool.

The finding that brain metastases from a wide spectrum of cellular origins also oxidize acetate, however, was not anticipated since organs that most frequently give rise to tumors that metastasize to the brain (lung, breast, kidney, and, melanoma) are not known to show significant ^{11}C-acetate uptake on PET. The data suggests that the ability to oxidize acetate is either a unique adaptation to the brain microenvironment or a more general property of tumor cells. In support of the latter possibility, several non-CNS tumors, including liver and prostate cancer, show avid differential ^{11}C-acetate uptake on PET relative to the normal organ (Ho et al., 2003; Oyama et al., 2002).

'Co-oxidation' of acetate and glucose was seen in all of the GBM and brain metastasis HOT models, raising the possibility that substrate co-oxidation might be an adaptive mechanism in rapidly proliferating tumors. It would ensure the availability of an adequate pool of carbons to generate CAC intermediates and support the high bioenergetic demands of growth while a large fraction of the glucose is being diverted to lactate. In this study there was no evidence of direct ^{13}C-glutamine oxidation in the orthotopic models, which may reflect differential substrate handling in brain tumors.

Normal plasma acetate levels in non-fasted humans range between 0.05 mM (Tollinger et al., 1979) and 0.18 mM (Skutches et al., 1979). Under normal resting conditions, circulating acetate levels may contribute up to 10–15% of the basal energy demands of brain astrocytes (Dienel and Cruz, 2006). Circulating free acetate is generated by fermentation of carbohydrates in the gut by commensal anaerobes and by the liver under ketogenic conditions (low glucose) as a final product of fatty acid oxidation or by ethanol metabolism in heavy drinkers (Jiang et al., 2013). It has recently been reported that 3 hours after oral administration of ^{13}C-inulin to mice, doublets of C4 glutamate and glutamine can be clearly resolved in brain by high-resolution magic angle spinning MR spectroscopy from brain uptake of circulating ^{13}C-labeled acetate (Frost et al., 2014). Moreover, the relative contribution of acetate to brain metabolism has been shown to increase following brain injury which limits glucose oxidation (Bartnik-Olson et al., 2010). This finding may be analogous to brain tumor regions with a paucity of active neurons and limited PDH activity

as a result of intratumoral hypoxia. Taken together, there is clear evidence that normal circulating acetate levels may be adequate to contribute to the metabolic demands of the tumor.

In order for the tumor cell to metabolize acetate, the cell must upregulate ACSS2, the enzyme critical for converting acetate to acetyl-coA, as shown in hepatoceullar carcinoma in the accompanying manuscript (Comerford et al., 2014). The increased expression of ACSS2 in GBM when compared to the lower grade gliomas supports the assertion that upregulation of this enzyme is linked to an increase in acetate oxidation by the tumor. Higher expression of ACSS2 is associated with shorter survival in the patients with low-grade gliomas, potentially identifying those tumors that are destined to transform to GBM more rapidly.

GBM neurospheres have been shown to be critically dependent on oxidative phosphorylation but not on inhibition of glycolysis (Janiszewska et al., 2012). This is consistent with our finding that inhibition of ACSS2 in the GBM neurospheres results in loss of clonogenicity and cell death and supports our hypothesis that ACSS2 is critical for supporting GBM viability. Moreover, the data from the genetically engineered glioma model show that mutations that drive AKT and ERK pathways (loss of PTEN and constitutive $BRAF^{V600E}$ activation) converge to increase ACSS2 expression (Figure 5). The most direct link between the enzyme and the cell's ability to oxidize acetate in the CAC was shown in ACSS2 null MEFs. Although this is a different system than glial cells, the finding that labeled glutamate from ^{13}C-acetate increased markedly in a time dependent manner in ACSS2 null MEFS when the WT ACSS2 was reintroduced into the cells is consistent with the wide range of tumor cell types that are able to oxidize acetate.

Recent evidence suggests that in order for tumor cells to adapt to the brain microenvironment, they must undergo unique genetic adaptations (Grassian et al., 2011; Valiente et al., 2014). In view of this formidable challenge, identification of a potentially druggable target, such as ACSS2, which appears to have little function in normal cells, offers unique advantages in therapy development. The current work and that of Comerford and colleagues underscores the value of *in vivo* studies in cancer metabolism. Having orthotopic tumor models of both GBM and a wide range of brain metastases that have been vigorously cross-validated with human data will enable rapid *in vivo* workup of novel small molecule inhibitors that target acetate metabolism, such as ACSS2. In addition, the feasibility of the ^{13}C-nutrient methodology in patients enables a host of follow up questions to be addressed from this work, including whether the ability to oxidize acetate is a property of early stage tumors or of the acquisition of metastatic potential. Rapid translation is a critical need for patients suffering from GBM and brain metastases where prognosis is measured in months.

EXPERIMENTAL PROCEDURES

Generation of Human Orthotopic Tumor (HOT) mouse models of GBM and brain metastases

Generation of the HOT models of GBM and brain metastases have been previously described (Marin-Valencia et al., 2012a). Briefly, tumor samples were obtained from

patients at the University of Texas Southwestern Medical Center at the time of craniotomy and tumor resection after written informed consent under an Institutional Review Board approved clinical protocol. All brain metabolic labeling experiments were performed in awake, alert mice following placement of an indwelling jugular venous catheter. For isolation of tumor and NT brain regions, the whole brains were cut into 1 mm coronal sections and microdissected to minimize contamination of tumor and NT regions.

Primary cell cultures

Primary astrocyte cultures were cultured as previously described (Bachoo et al., 2002). They were isolated from genetically engineered, multiallele conditional mice with the following mutations as single or combination ($p53^{f/f}$, $PTEN^{f/f}$ and $_{LSL}BRAF^{V600E}$). Primary GBM neurospheres were isolated and maintained under standard neurosphere culture conditions.

Infusions of ^{13}C-Labeled Nutrients and Dissection of Brains and Tumors

Mouse studies—Tracer studies in the HOT mice were performed as previously described (Marin-Valencia et al., 2012c). Mice were infused with [1,6-^{13}C] glucose (1-^{13}C, 99% enriched; 6-^{13}C, 99% enriched, Sigma-Aldrich Isotec, Miamisburg, OH) and [1,2-^{13}C] acetate (1-^{13}C, 99% enriched; 2-^{13}C, 99% enriched, Cambridge Isotope Laboratories, Cambridge, MA) as a bolus of 0.6 mg/g of body weight for each tracer (in 0.3 ml of saline) infused over 1 min, followed by a continuous infusion of 0.0138 mg/g of body weight/min for each tracer (in 0.431 ml of saline) at 150 μL/h during 150 min. For the experiments using glutamine, mice were infused with [U-^{13}C] glutamine (95% enriched, Sigma-Aldrich Isotec, Miamisburg, OH) as a bolus of 0.28 mg/g of body weight for each tracer (in 0.3 ml of saline) infused over 1 min, followed by a continuous infusion of 0.005 mg/g of body weight/min for each tracer (in 0.45 ml of saline) at 150 μL/h during 180 min.

Human studies—Patients were enrolled in an UT Southwestern Medical Center IRB approved protocol to infuse ^{13}C-isotopes (glucose and acetate). For [1,2-^{13}C]acetate infusion, patients were dosed with 6 mg/kg/min for 10 minutes followed by 3 mg/kg/min for 2–3 hours. Patient recruitment and consent, as well as blood and tumor sampling have been previously described (Maher et al., 2012).

^{13}C NMR Spectroscopy

Proton-decoupled ^{13}C spectra of tumor and NT brain extracts were acquired at 150 MHz for ^{13}C, on Agilent VNMRS Direct Drive Console using 3mm broadband NMR probe (Agilent Technologies, Palo Alto, CA). Various ^{13}C resonances were assigned based on chemical shift position referenced to the lactate C3 singlet at 20.8 ppm. Relative peak areas of the multiplets were obtained using ACD NMR Processor as previously described (Maher et al., 2012; Malloy et al., 1987, 1990a).

Immunohistochemistry (IHC)

Paraffin-embedded GBM and brain metastasis specimens were obtained from the Division of Neuropathology at UT Southwestern Medical Center. Formalin fixed paraffin embedded (FFPE) 4 micron sections were used for IHC. The primary antibodies and their dilutions

were as follows: rabbit monoclonal ER (Ventana, Cat.Lo.790-4296, 1:100 Dilution), rabbit monoclonal PR (Ventana, Cat.Lo.790-4325, 1:200 Dilution), rabbit monoclonal HER 2 (Ventana, Cat.Lo.790-2991, 1:200 Dilution), and rabbit polyclonal ACSS2 (Cell Signaling, Cat.Lo.3658S, 1:200 Dilution).

RNA Isolation, cDNA preparation and qRT-PCR

RNA was isolated from cells in culture using an RNA Isolation Kit (Qiagen RNeasy Mini Kit) following the manufacturer's protocol. cDNA was generated using the iScript™ cDNA Synthesis Kit (BioRad). Quantitative real time PCR using iTaq™ SYBR® Green Supermix with ROX (Bio-Rad) was performed on a StepOnePlus™ Real-Time PCR Systems (Applied Biosystems).

Molecular analysis

DNA was prepared according to standard methods and QPCR for EGFR, ALK, BRAF V600E, PTEN, p16, p19 was done with standard primer sets for these genes.

Plasma acetate measurement

Plasma acetate was measured using standard manufacturer's protocol (Biovision Colorimetric Assay Kit, Cat# K658). Briefly, 1ul of the diluted clear filtrate plasma was used for experimental samples. The reaction was performed at room temperature for 40 minutes and optical reading was taken at 450 nm using spectrophotometer. The unknown sample concentration was calculated from the standard curve.

Metabolite extraction and LC-MS/MS

Cells were seeded on 6cm plate to 70%–80% confluency. After two washes in PBS, cells were cultured with glutamine starvation medium (DMEM w/o glucose and glutamine (Cat # D5030, Sigma-Aldrich), 3.7g/l Sodium bicarbonate, 5.9g/l HEPES, 20mM glucose, 10% FBS) and 2mM sodium [1,2-^{13}C]acetate (Cat# CLM-440-1, Cambridge Isotope Laboratories) was added to the cells and metabolites were extracted 0hr, 0.5hr, 1hr, 2hr after acetate addition. After washing with ice cold PBS, 500 μl of ice-cold 50% HPLC grade methanol was added to the cells. The plate was floated on liquid nitrogen immediately until the methanol was frozen. The plate was removed from the liquid nitrogen and scraped until the methanol was thawed. The suspension was then passed through 10 freeze/thaw cycles using a bead beater and liquid nitrogen and then centrifuged at 16,000 g at 4°C for 10 min. Supernatants were transferred to a new tube and dried down. Metabolites were re-suspended in 140 μl TBA buffer (5mM tributylammonium acetate pH 5.0) and vortexed for 15 min. The solution was placed on ice for 30 min and then centrifuged at max speed for 5 min. The supernatants were transferred to a new tube, placed on ice for 30 min and then centrifuged at max speed for 5 min. The supernatants were then processed for LC-MS/MS analysis as described previously using a water/methanol gradient with TBA as the ion pairing agent. A negative mode method targeting labeled glutamate was established based on examining the pattern of incorporation of labeled acetate carbons into glutamate, via entry of cytosolic acetyl-CoA into the TCA cycle. Analysis of the MS/MS fragmentation pattern for glutamate

established two MRM pairs (148/103 and 148/130) for detection of [1,2-^{13}C]acetate conversion to M+2 glutamate (Tu et al., 2007).

Retroviral studies

ACSS2-shRNA-expressing retroviral plasmid with a puromycin selection gene was used for knockdown studies. We used a scrambled shRNA as control. Retroviral containing media was obtained from transfected 293T cells and added to GBM cells followed by puromycin selection.

Statistical Analysis

All pooled results are reported as mean+/−SEM. For the evaluation of the acetate:glucose ratio between tumor and NT brain, a paired t-test was used.

For ACSS2 IHC evaluation, the immunostained TMA slides were scored manually by assigning to each core a value for ACSS2 staining intensity on a scale of 0–3 and a value representing the proportion of tumor cells staining on a scale of 0–100%. These two values (intensity and percent positive cells) were then multiplied to obtain a histoscore (range, 0–300), which was used in further analyses. ACSS2 histoscores were dichotomized to high and low at the median. Kaplan–Meier survival curves were generated and compared with the Mantel-Cox (logrank) test using GraphPad Prism version 6.01 software (GraphPad, La Jolla, CA, USA).

Supplementary Material

Refer to Web version on PubMed Central for supplementary material.

ACKNOWLEDGEMENTS

We thank Craig Malloy and Dean Sherry for analytical assistance with the NMR spectral data, critical reading of the manuscript and helpful discussions. We thank Sarah McNeil and Christie Sheppard for significant contributions to the patient studies, and Dinesh Ramesh for assistance with figures. This work was supported by grants from Cancer Prevention Research Institute of Texas RP101243 to CRM, RJD, EAM, and RMB, NIH 5R01CA154843-03 to EM, NIH Resource Grant EB015908 to CRM, NIH R01 CA157996 to RJD, and Simmons Cancer Center NIH support grant 5P30 CA142543-04. The work was also supported by development funds from The Annette G. Strauss Center for Neuro-Oncology, The Miller Family Fund, The Glady Jo Salvino Fund at UT Southwestern Medical Center and the Kenny Can Foundation, Dallas, Texas.

REFERENCES

Bachoo RM, Maher EA, Ligon KL, Sharpless NE, Chan SS, You MJ, Tang Y, DeFrances J, Stover E, Weissleder R, et al. Epidermal growth factor receptor and Ink4a/Arf: convergent mechanisms governing terminal differentiation and transformation along the neural stem cell to astrocyte axis. Cancer Cell. 2002; 1:269–277. [PubMed: 12086863]

Bartnik-Olson BL, Oyoyo U, Hovda DA, Sutton RL. Astrocyte oxidative metabolism and metabolite trafficking after fluid percussion brain injury in adult rats. Journal of neurotrauma. 2010; 27:2191–2202. [PubMed: 20939699]

Brennan CW, Verhaak RG, McKenna A, Campos B, Noushmehr H, Salama SR, Zheng S, Chakravarty D, Sanborn JZ, Berman SH, et al. The somatic genomic landscape of glioblastoma. Cell. 2013; 155:462–477. [PubMed: 24120142]

Comerford S, Huang Z, Du X, Wang Y, Cai L, Witkiewicz A, Walters H, Tantawy M, Fu A, Manning H, et al. Acetate Dependence of Tumors. Cell. 2014 In Press.

Deelchand DK, Nelson C, Shestov AA, Ugurbil K, Henry PG. Simultaneous measurement of neuronal and glial metabolism in rat brain in vivo using co-infusion of [1,6-$^{13}C_2$]glucose and [1,2-$^{13}C_2$]acetate. J Magn Reson. 2009; 196:157–163. [PubMed: 19027334]

Dienel GA, Cruz NF. Astrocyte activation in working brain: energy supplied by minor substrates. Neurochemistry international. 2006; 48:586–595. [PubMed: 16513214]

Ebert D, Haller RG, Walton ME. Energy contribution of octanoate to intact rat brain metabolism measured by 13C nuclear magnetic resonance spectroscopy. J Neurosci. 2003; 23:5928–5935. [PubMed: 12843297]

Fine HA. Bevacizumab in glioblastoma--still much to learn. N Engl J Med. 2014; 370:764–765. [PubMed: 24552324]

Frost G, Sleeth ML, Sahuri-Arisoylu M, Lizarbe B, Cerdan S, Brody L, Anastasovska J, Ghourab S, Hankir M, Zhang S, et al. The short-chain fatty acid acetate reduces appetite via a central homeostatic mechanism. Nature communications. 2014; 5:3611.

Grassian AR, Metallo CM, Coloff JL, Stephanopoulos G, Brugge JS. Erk regulation of pyruvate dehydrogenase flux through PDK4 modulates cell proliferation. Genes Dev. 2011; 25:1716–1733. [PubMed: 21852536]

Ho CL, Yu SC, Yeung DW. 11C-acetate PET imaging in hepatocellular carcinoma and other liver masses. Journal of nuclear medicine : official publication, Society of Nuclear Medicine. 2003; 44:213–221.

Janiszewska M, Suva ML, Riggi N, Houtkooper RH, Auwerx J, Clement-Schatlo V, Radovanovic I, Rheinbay E, Provero P, Stamenkovic I. Imp2 controls oxidative phosphorylation and is crucial for preserving glioblastoma cancer stem cells. Genes Dev. 2012; 26:1926–1944. [PubMed: 22899010]

Jiang L, Gulanski BI, De Feyter HM, Weinzimer SA, Pittman B, Guidone E, Koretski J, Harman S, Petrakis IL, Krystal JH, et al. Increased brain uptake and oxidation of acetate in heavy drinkers. J Clin Invest. 2013; 123:1605–1614. [PubMed: 23478412]

Lu-Emerson C, Eichler AF. Brain metastases. Continuum. 2012; 18:295–311. [PubMed: 22810128]

Maher EA, Marin-Valencia I, Bachoo RM, Mashimo T, Raisanen J, Hatanpaa KJ, Jindal A, Jeffrey FM, Choi C, Madden C, et al. Metabolism of [U-13 C]glucose in human brain tumors in vivo. NMR Biomed. 2012; 25:1234–1244. [PubMed: 22419606]

Malloy CR, Sherry AD, Jeffrey FM. Carbon flux through citric acid cycle pathways in perfused heart by 13C NMR spectroscopy. FEBS Lett. 1987; 212:58–62. [PubMed: 2879743]

Malloy CR, Sherry AD, Jeffrey FM. Evaluation of carbon flux and substrate selection through alternate pathways involving the citric acid cycle of the heart by 13C NMR spectroscopy. J Biol Chem. 1988; 263:6964–6971. [PubMed: 3284880]

Malloy CR, Sherry AD, Jeffrey FM. Analysis of tricarboxylic acid cycle of the heart using 13C isotope isomers. Am J Physiol. 1990a; 259:H987–995. [PubMed: 1975735]

Malloy CR, Thompson JR, Jeffrey FM, Sherry AD. Contribution of exogenous substrates to acetyl coenzyme A: measurement by 13C NMR under non-steady-state conditions. Biochemistry. 1990b; 29:6756–6761. [PubMed: 1975750]

Marin-Valencia I, Cho SK, Rakheja D, Hatanpaa KJ, Kapur P, Mashimo T, Jindal A, Vemireddy V, Good LB, Raisanen J, et al. Glucose metabolism via the pentose phosphate pathway, glycolysis and Krebs cycle in an orthotopic mouse model of human brain tumors. NMR Biomed. 2012a; 25:1177–1186. [PubMed: 22383401]

Marin-Valencia I, Good LB, Ma Q, Malloy CR, Patel MS, Pascual JM. Cortical metabolism in pyruvate dehydrogenase deficiency revealed by ex vivo multiplet (13)C NMR of the adult mouse brain. Neurochemistry international. 2012b; 61:1036–1043. [PubMed: 22884585]

Marin-Valencia I, Yang C, Mashimo T, Cho S, Baek H, Yang XL, Rajagopalan KN, Maddie M, Vemireddy V, Zhao Z, et al. Analysis of tumor metabolism reveals mitochondrial glucose oxidation in genetically diverse human glioblastomas in the mouse brain in vivo. Cell Metab. 2012c; 15:827–837. [PubMed: 22682223]

Owonikoko TK, Arbiser J, Zelnak A, Shu HK, Shim H, Robin AM, Kalkanis SN, Whitsett TG, Salhia B, Tran NL, et al. Current approaches to the treatment of metastatic brain tumours. Nat Rev Clin Oncol. 2014

Oyama N, Akino H, Kanamaru H, Suzuki Y, Muramoto S, Yonekura Y, Sadato N, Yamamoto K, Okada K. 11C-acetate PET imaging of prostate cancer. Journal of nuclear medicine : official publication, Society of Nuclear Medicine. 2002; 43:181–186.

Sagiyama K, Mashimo T, Togao O, Vemireddy V, Hatanpaa KJ, Maher EA, Mickey BE, Pan E, Sherry AD, Bachoo RM, et al. In vivo chemical exchange saturation transfer imaging allows early detection of a therapeutic response in glioblastoma. Proc Natl Acad Sci U S A. 2014; 111:4542–4547. [PubMed: 24616497]

Schurr, A. Neuronal energy requirements. In: Walz, W., editor. The neuronal environment: brain homeostasis in health and disease. New Jersey: Humana Press; 2001. p. 25-54.

Sherry AD, Malloy CR, Zhao P, Thompson JR. Alterations in substrate utilization in the reperfused myocardium: a direct analysis by 13C NMR. Biochemistry. 1992; 31:4833–4837. [PubMed: 1350466]

Skutches CL, Holroyde CP, Myers RN, Paul P, Reichard GA. Plasma acetate turnover and oxidation. J Clin Invest. 1979; 64:708–713. [PubMed: 468985]

Taylor A, McLean M, Morris P, Bachelard H. Approaches to studies on neuronal/glial relationships by 13C-MRS analysis. Developmental neuroscience. 1996; 18:434–442. [PubMed: 8940616]

Tollinger CD, Vreman HJ, Weiner MW. Measurement of acetate in human blood by gas chromatography: effects of sample preparation, feeding, and various diseases. Clinical chemistry. 1979; 25:1787–1790. [PubMed: 476928]

Tu BP, Mohler RE, Liu JC, Dombek KM, Young ET, Synovec RE, McKnight SL. Cyclic changes in metabolic state during the life of a yeast cell. Proc Natl Acad Sci U S A. 2007; 104:16886–16891. [PubMed: 17940006]

Valiente M, Obenauf AC, Jin X, Chen Q, Zhang XH, Lee DJ, Chaft JE, Kris MG, Huse JT, Brogi E, et al. Serpins promote cancer cell survival and vascular co-option in brain metastasis. Cell. 2014; 156:1002–1016. [PubMed: 24581498]

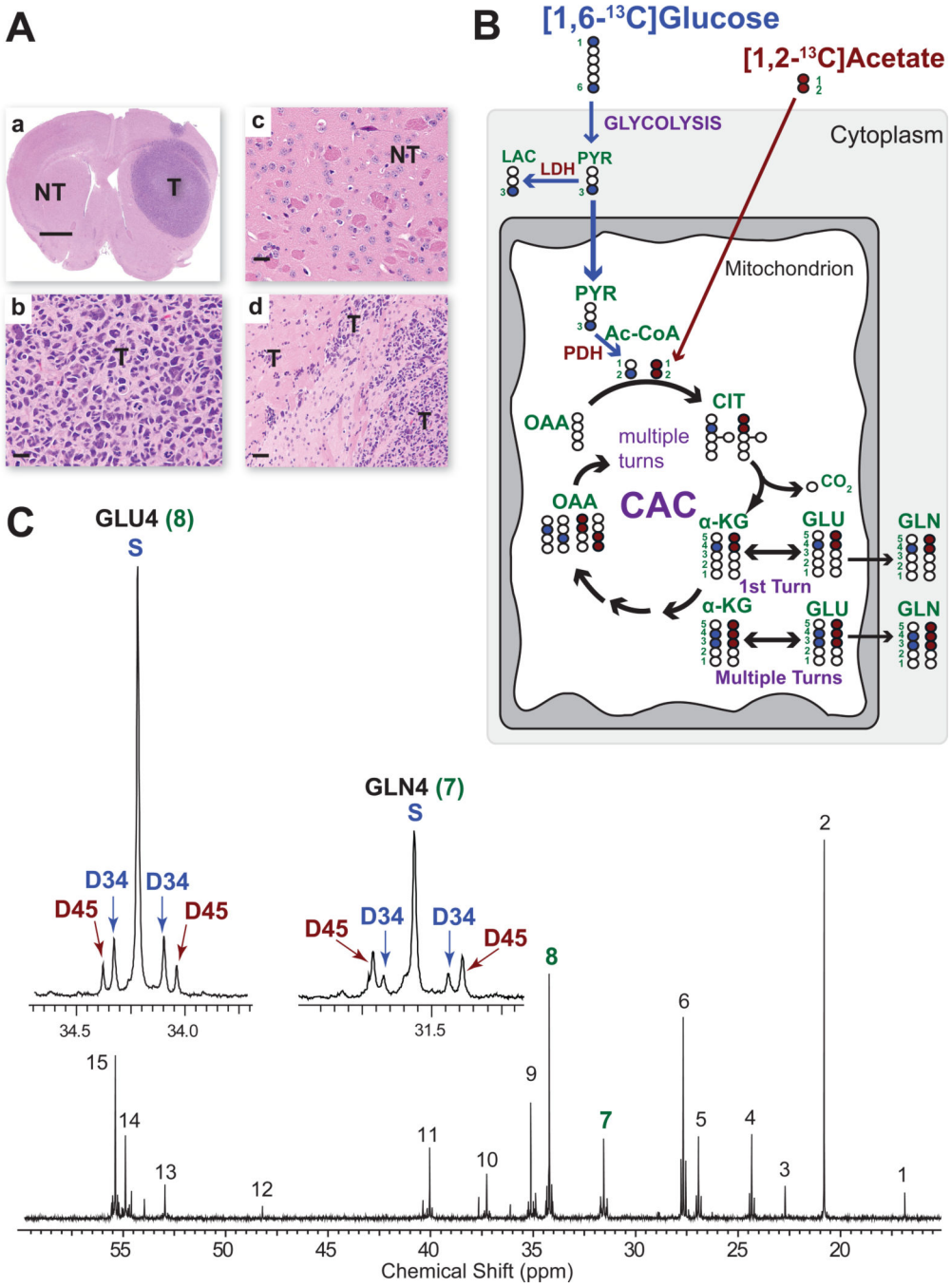

Figure 1. Metabolism of co-infused [1,6-^{13}C]glucose and [1,2-^{13}C]acetate

(A) Low power hematoxylin & eosin (H&E) of a GBM HOT mouse brain at the time of co-infusion. (a) A large tumor (T) mass is seen in the right hemisphere. The left hemisphere is designated non-tumor (NT) brain. Scale bar 0.3 cm. High power images from (b) tumor (T) and (c) NT brain (scale bars 10 μm), and (d) tumor infiltrating brain at the edge of the mass (scale bar 20 μm). (B) Schema showing the fate of individual carbons from infused [1,6-^{13}C]glucose (blue filled circles-^{13}C) and [1,2-^{13}C]acetate (red filled circles-^{13}C) through the first turn of the CAC and labeling in α-KG, GLU and GLN after multiple turns.

Open circles ^{12}C. Numbers refer to carbon positions. Abbreviations: LAC, lactate; Ac-CoA, acetyl CoA; CIT, citrate; α-KG, α- ketoglutarate; GLU, glutamate; GLN, glutamine; OAA, oxaloacetate; PDH, pyruvate dehydrogenase; LDH, lactate dehydrogenase; PYR, pyruvate. (C) ^{13}C-NMR spectrum from NT brain after co-infusion. Insets are GLU4 and GLN4. Singlet (S) and doublet 3,4 (D34) in blue are generated from ^{13}C-glucose metabolism and doublets 4,5 (D45) in red are generated from ^{13}C-acetate metabolism. The color scheme is the same in all figures. Chemical shift assignments: 1, Alanine C3; 2, Lactate C3; 3, N-acetylaspartate C6; 4, GABA C3; 5, Glutamine C3; 6, Glutamate C3; 7, Glutamine C4; 8, Glutamate C4; 9, GABA C2; 10, Aspartate C3; 11, GABA C4; 12, Taurine (?); 13, Aspartate C2; 14, Glutamine C2; 15, Glutamate C2.

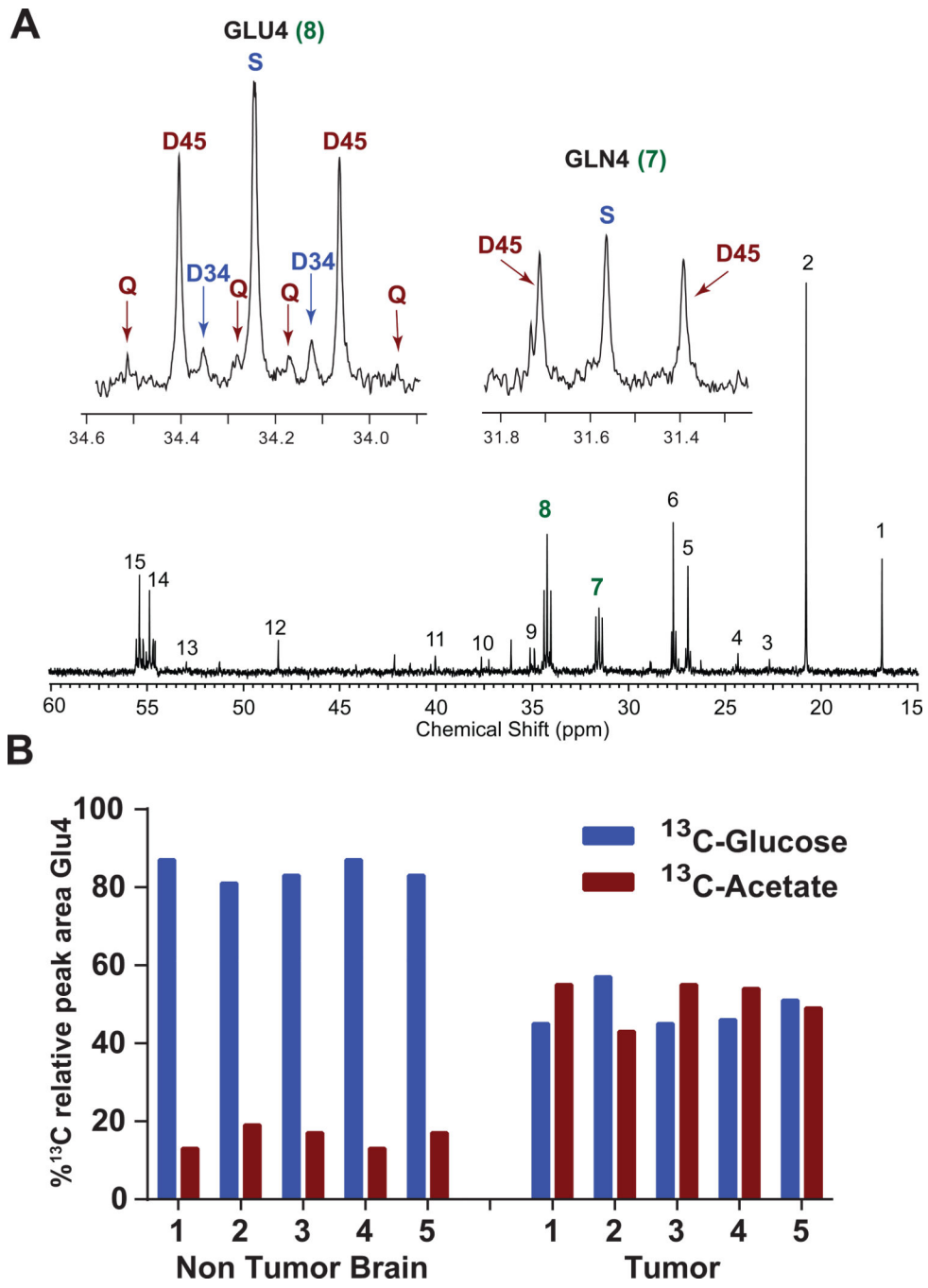

Figure 2. Metabolism of co-infused [1,6-^{13}C]glucose and [1,2-^{13}C]acetate in GBM vs NT brain

(A) ^{13}C-NMR GBM tumor spectrum after co-infusion. Inserts are GLU4 and GLN4. Chemical shift assignments same as in Figure 1. (B) Relative percent labeling of GLU4 by acetate and glucose in 5 replicates of NT brain and T from UT-GBM1. Peak areas in GLU4 were measured from the ^{13}C-NMR spectra. The contribution of ^{13}C-glucose (S+D34) (blue bars) and ^{13}C-acetate (D45+Q) (red bars) are expressed as percent of total peak area in GLU4. See also Figure S1.

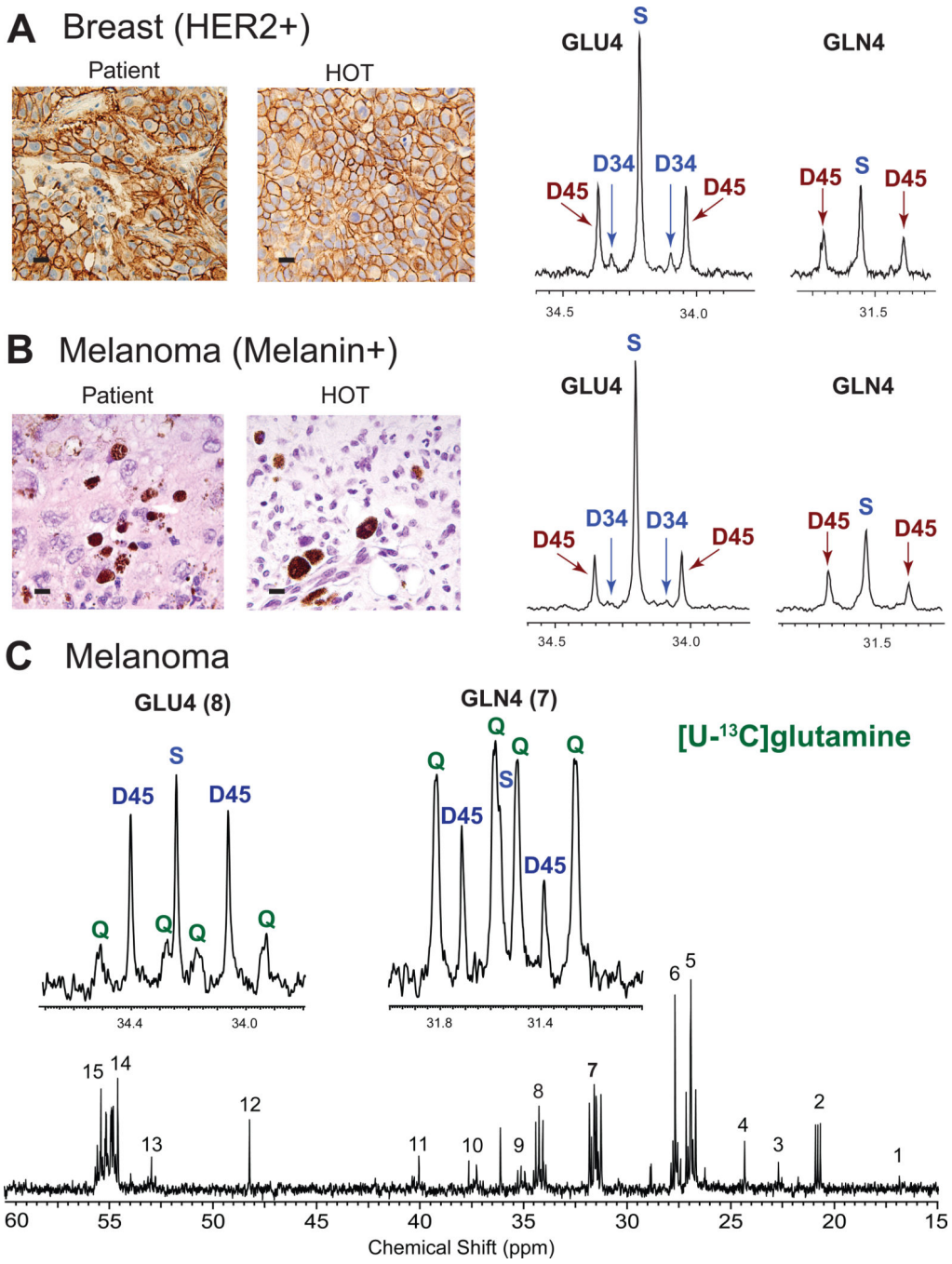

Figure 3. Oxidation of ^{13}C-acetate but not ^{13}C-glutamine in brain metastases

Co-infusion of [1,6-^{13}C]glucose and [1,2-^{13}C]acetate in HOT models from (A) Breast cancer brain metastasis (ER+, PR+, HER2+) and (B) Melanoma (BRAF^{V600E} mutant). Scale bars 10 μm. Patient tumor (left panel) is compared with the HOT mouse tumor generated from the same patient tumor (right panel) for HER2 in breast (A) and melanin in melanoma (B). The GLU4 and GLN4 ^{13}C-NMR profiles from the HOT tumors show similar labeling patterns with prominent D45 generated from ^{13}C-acetate oxidation. The presence of S and D34 indicates that ^{13}C-glucose was oxidized simultaneously. Note the similar pattern in

GLN4 (prominent D45) in both tumor spectra. (C) Infusion of [U-^{13}C]glutamine in the melanoma HOT model. Insets are GLU4 and GLN4. Note the different labeling pattern in GLU4 and GLN4. Prominent labeling was not detected in aspartate (C3 in position 10 and C2 in position 13 in the full spectrum) or malate (MAL) (unlabeled). See also Figure S2.

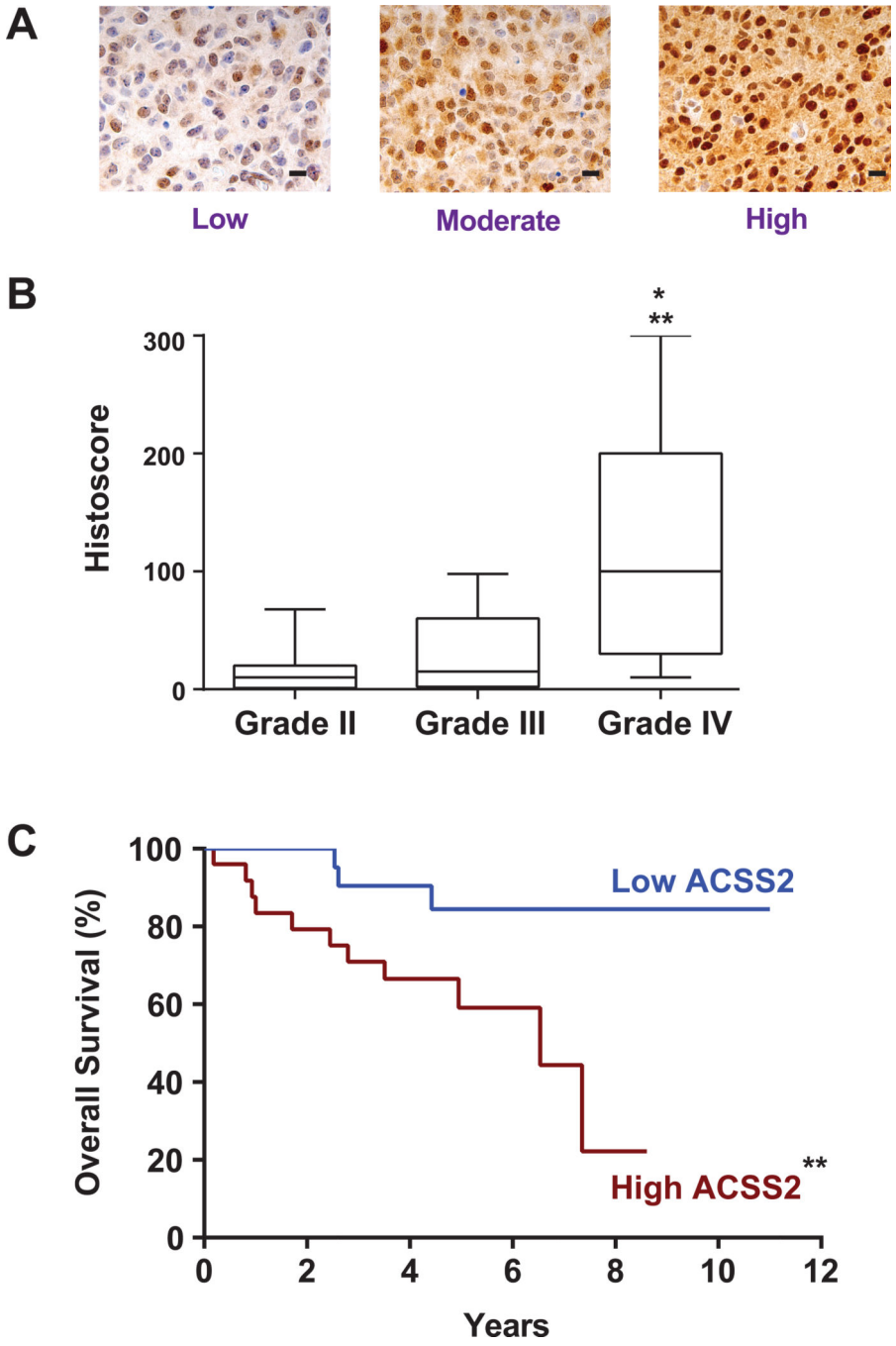

Figure 4. Immunoreactivity to ACSS2 is correlated with glioma grade and survival of grade II and II gliomas

(A) Representative sections from glioma TMA showing the range of ACSS2 staining. Low – fewer than 50% of tumor cells are positive and intensity of staining is 1 (scale 0–3); Moderate – 75% positive, intensity 1–3; High – 100% positive and intensity 2–3.

(B) Box and whisker plot of ACSS2 histoscore for WHO Grades II, III, and IV gliomas. ** Grade II vs Grade IV ($p<0.001$) and *Grade III vs Grade IV ($p<0.01$).

(C) Kaplan-Meier curve of Grade II and III astrocytomas and oligoastrocytomas. High vs low ACSS2 staining (n=25 each group) based on the median histoscore. **p<0.001 survival difference. See also Figure S3A for ACSS2 immunoreactivity in brain metastasis HOT lines.

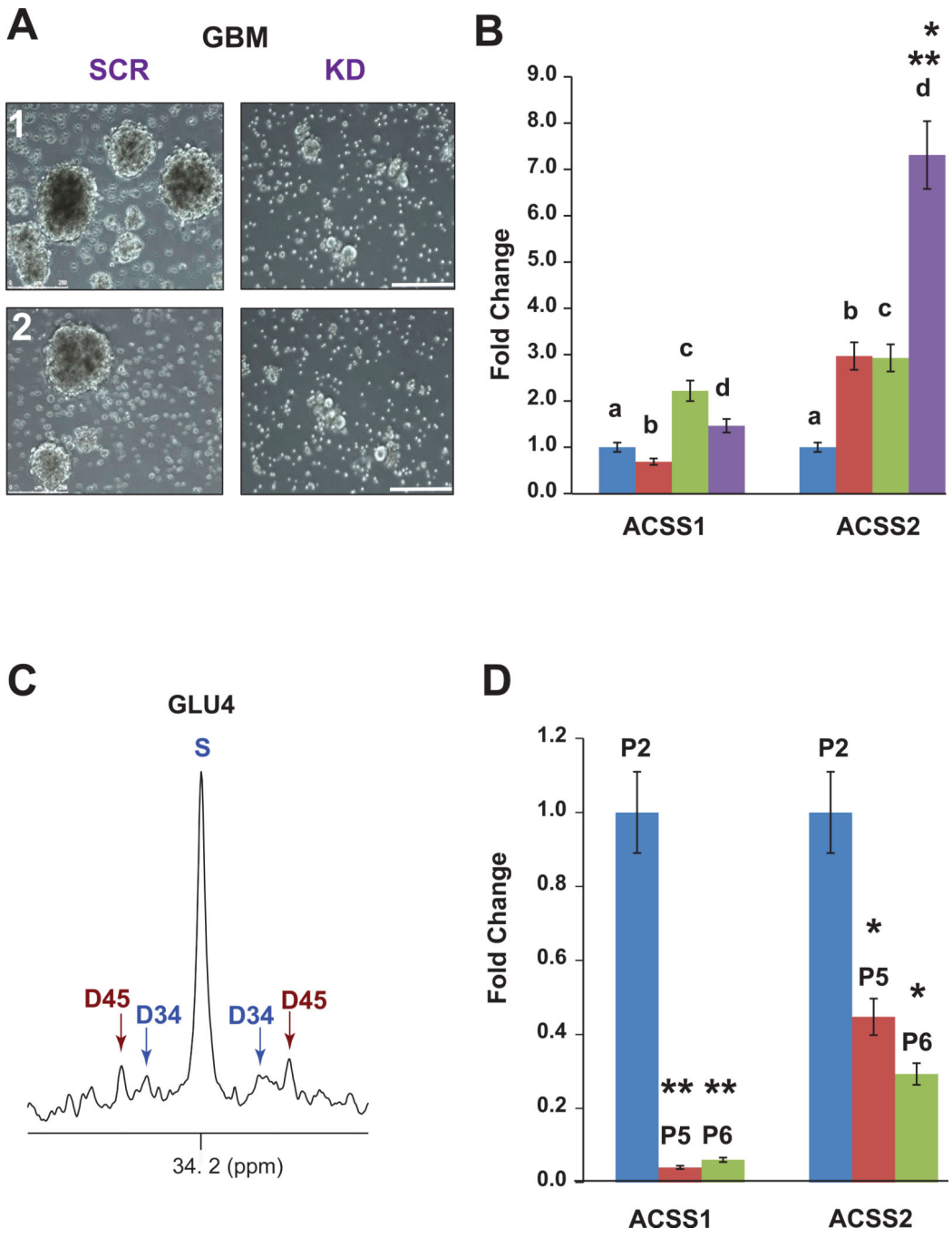

Figure 5. Expression of ACSS2 is linked to GBM growth and malignant potential

(A) Comparison of primary GBM cultures infected with retroviruses expressing ACSS2 shRNAi (KD) or scrambled shRNAi (SCR). Two independent cultures are shown. Neurospheres are visible in the SCR cultures but not in KD cultures. Scale bars 250 μm. (B) Fold change (qRT-PCR) of ACSS1 and ACSS2 mRNA in primary conditional (floxed) astrocyte cultures after infection with adenocre to produce (a) p53−/−, (b) p53−/−, PTEN−/−, (c) p53+/−, PTEN−/−, $BRAF^{V600E}$ and (d) p53−/−, PTEN−/−, $BRAF^{V600E}$. *p<0.01 vs b or c; **p<0.001 vs a. **C**. Glutamate C4 multiplets from ^{13}C-NMR spectrum of an

intracranial tumor arising from p53−/−, PTEN−/−, $BRAF^{V600E}$ astrocytes after co-infusion of ^{13}C-acetate and ^{13}C-glucose. **D**. Fold change (qRT-PCR) of ACSS1 and ACSS2 mRNA in primary astrocytes in culture at passages 2 (P2), 5 (P5), and 6 (P6). *p<0.01, ** p<0.005 vs P2. See also Figure S3B.

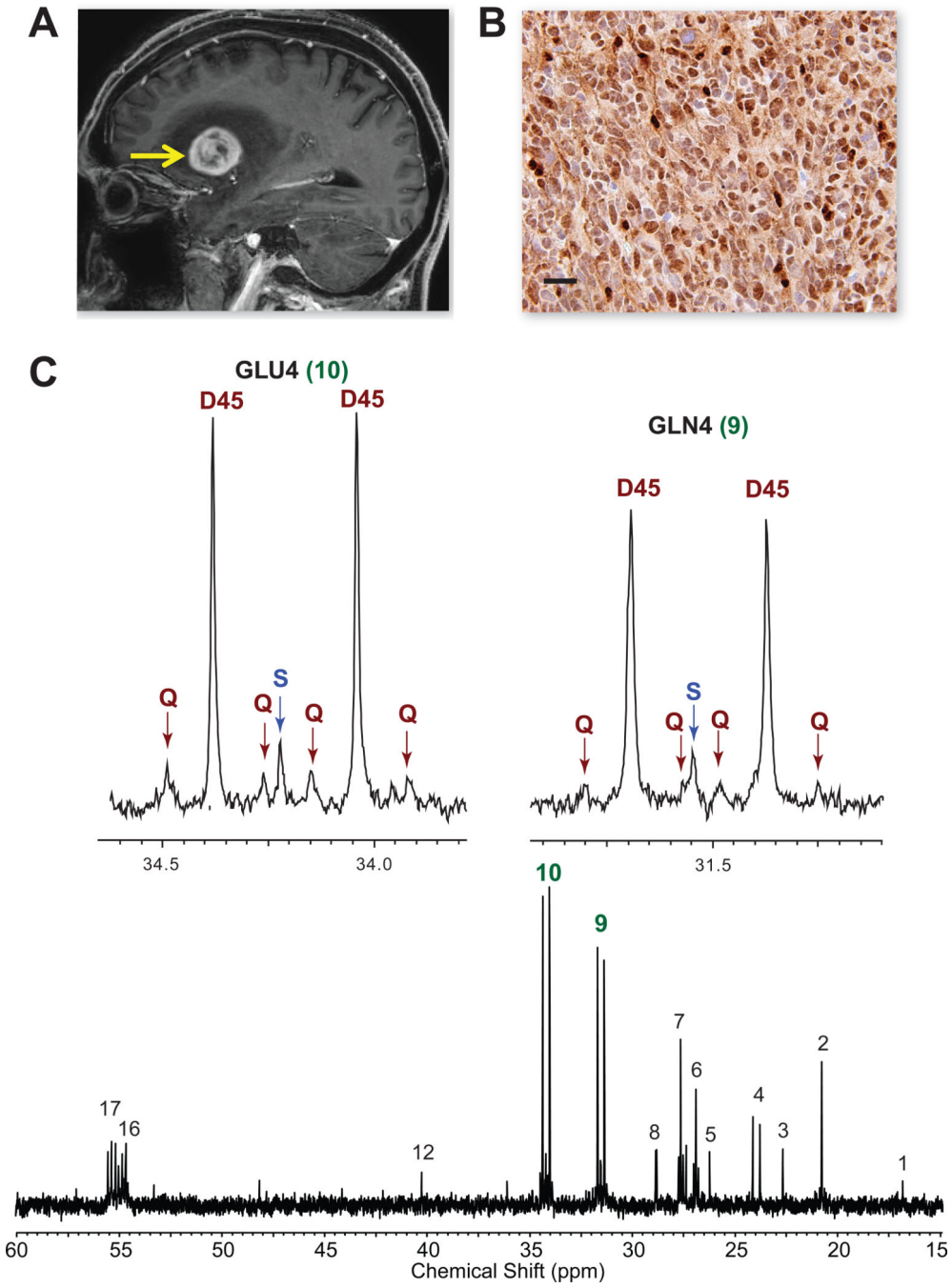

Figure 6. Oxidation of [1,2^{13}C]-acetate in a patient with GBM

(A) Pre-operative sagittal image from gadolinium-enhanced MRI shows a large enhancing tumor in the left frontotemporal region (arrow). (B) Strong ACSS2 immunoreactivity in the tumor. Scale bar 10 μm. (C) ^{13}C-NMR spectrum with GLU4 and GLN4 insets. Note the prominent D45 and Qs reflecting robust ^{13}C-acetate oxidation. Abbreviations same as Figure 2. Chemical shift assignments: 1, Alanine C3; 2, Lactate C3; 3, N-acetylaspartate C6; 4, Acetate C2; 5, unassigned; 6, Glutamine C3; 7, Glutamate C3; 8, unassigned; 9,

Glutamine C4; 10, Glutamate C4; 12, N-acetylaspartate C3; 16, Glutamine C2; 17, Glutamate C2.

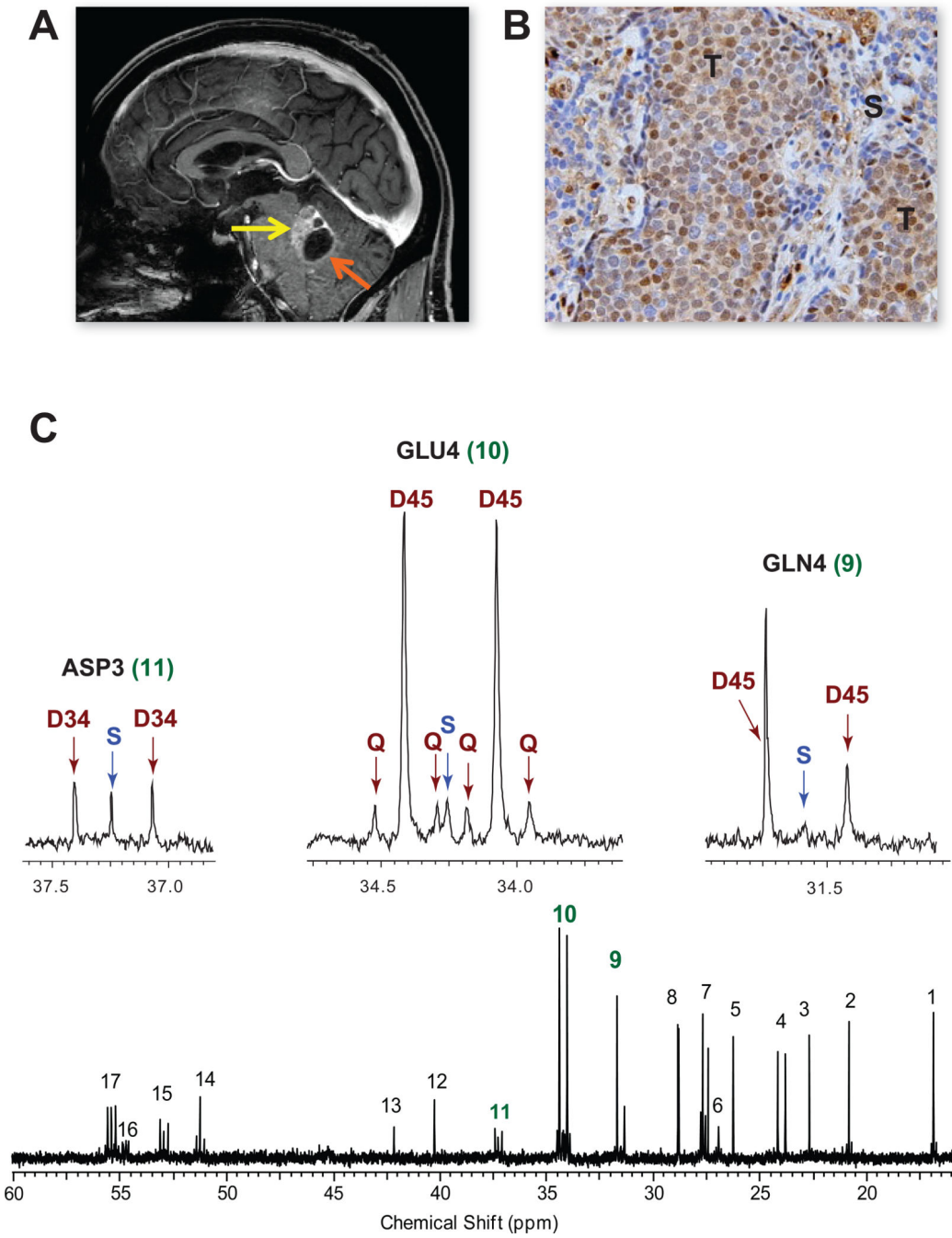

Figure 7. Infusion of [1,2^{13}C]acetate in a patient with a non-small cell lung cancer brain metastasis

(A) Pre-operative MRI, sagittal image, shows a gadolinium-enhancing tumor in the left cerebellum (yellow arrow) with a cystic component (orange arrow). (B) Moderate ACSS2 immunoreactivity in the tumor (T) with lack of staining in the surrounding stroma (S). Scale bar 10 um. (C) ^{13}C-NMR spectrum with GLU4, GLN4 and ASP3 insets. Abbreviations same as Figure 2. Chemical shift assignments same as in Figure 6 with the addition of 11,

Aspartate C3; 13, Glycine C2; 14, Alanine C2; and 15, Aspartate C2. See also Figure S4 for ^{13}C-spectra from 2 additional patient tumors.